Zhou et al. Nanoscale Research Letters (2017) 12:629
DOI 10.1186/s11671-017-2392-2

Nanoscale Research Letters

NANO EXPRESS Open Access

A Resumable Fluorescent Probe BHN-Fe_3O_4@SiO_2 Hybrid Nanostructure for Fe^{3+} and its Application in Bioimaging

Xi Zhou[1], Yujiao Wang[1], Qi Peng[2] and Weisheng Liu[1*]

Abstract

A multifunctional fluorescent probe BHN-Fe_3O_4@SiO_2 nanostructure for Fe^{3+} was designed and developed. It has a good selective response to Fe^{3+} with fluorescence quenching and can be recycled using an external magnetic field. With adding EDTA (2.5×10^{-5} M) to the consequent product Fe^{3+}-BHN-Fe_3O_4@SiO_2, Fe^{3+} can be removed from the complex, and its fluorescence probing ability recovers, which means that this constituted on-off type fluorescence probe could be reversed and reused. At the same time, the probe has been successfully applied for quantitatively detecting Fe^{3+} in a linear mode with a low limit of detection 1.25×10^{-8} M. Furthermore, the BHN-Fe_3O_4@SiO_2 nanostructure probe is successfully used to detect Fe^{3+} in living HeLa cells, which shows its great potential in bioimaging detection.

Keywords: Fluorescent probe, Resumable, Hybrid nanostructure, Fe^{3+}, Bioimaging

Background

The development of new methods to detect all kinds of small molecules and ions has become an important task for scientific researchers. As one of the indispensable important metal ions in metabolic processes, Fe^{3+} plays an essential and crucial role in a variety of biological processes such as brain function and pathology, gene transcription, immune function, and mammalian reproduction [1–9]. The medical investigations indicate that the metabolic or biological processes are normal for the proper functioning of all living cells only when the Fe^{3+} concentration is in a suitable range. When Fe^{3+} concentration in a living body deviates from its suitable range, some diseases or serious disorders can be induced in the metabolic or biological processes [10–12]. Even though a variety of detection methods has been developed to detect Fe^{3+} [13–15], fluorescent technique is the more effective and powerful method, because of their operational simplicity, high sensitivity and selectivity, and low detection limit [16–20].

In these molecule-based fluorescent probes, some problems relative to the safety, the recyclability, and the reusability have not been solved. For example, as pointed out in reference [21], the employed small molecules are toxic. These deficiencies exhibited in the molecule-based fluorescent probes completely limit the probes entering into a practical application. To conquer the challenge of safety in the above fluorescent probes for Fe^{3+}, another technical approach is proposed by using inorganic supports incorporated with small molecular fluorescent probes. In such new approach, it is known that the inorganic materials such as magnetic nanoparticles, metal nanoparticles, nanotubes, and mesoporous silica can be used in the design of the fluorescent probes [22–24]. Among all these inorganic materials, magnetic silica core-shell Fe_3O_4@SiO_2 nanoparticles have advantages of their low toxicity, high biocompatibility, simply separation via external magnetic field, and large surface area that can be grafted by fluorescent probes over other materials in the molecule or ion recognition and separation areas [25–27]. Hence, this new approach provides us a possible way to realize the application for detecting Fe^{3+}, especially in the safety with low toxicity and high biocompatibility.

* Correspondence: liuws@lzu.edu.cn
[1]Key Laboratory of Nonferrous Metals Chemistry and Resources Utilization of Gansu Province, State Key Laboratory of Applied Organic Chemistry, College of Chemistry and Chemical Engineering, Lanzhou University, Lanzhou 730000, China
Full list of author information is available at the end of the article

In this work, a kind of multifunctional magnetic BHN-Fe_3O_4@SiO_2 nanostructure fluorescent sensor for Fe^{3+} was designed and synthesized. It has a good sensitive and selective response to Fe^{3+} with remarkably fluorescence quenching in CH_3CN/H_2O (1:1, *v*/*v*) at room temperature. By applying an external magnetic field, the probe can be separated from the solution. When adding EDTA to the system, Fe^{3+} can be removed from the complex with fluorescence intensity recovery. Furthermore, the confocal fluorescence imaging using HeLa cells showed that the probe could be applied to detect Fe^{3+} in living cells. Hence, the obtained BHN-Fe_3O_4@SiO_2 exhibits excellent selectivity, water solubility, reversibility, and recyclability, which benefits to the detection of Fe^{3+}.

Methods/Experimental

Synthesis of Fe_3O_4@SiO_2 Nanoparticles

Fe_3O_4 magnetite nanoparticles were synthesized according to reference [28]. They were further coated with a thin silica layer by means of a modified Stöber method [29] to obtain stable Fe_3O_4@SiO_2. Tetraethyl orthosilicate (TEOS) was hydrolyzed with magnetite nanoparticles as seeds in ethanol/water mixture. The resulting Fe_3O_4@SiO_2 nanoparticles with an average diameter of 50–60 nm were used as the carriers of fluorescent sensor nanoparticles.

Synthesis of BHN-Fe_3O_4@SiO_2 Nanostructure

N-butyl-4-bis(2-hydroxyethyl) amino-1,8-naphthalimide (BHN) is synthesized according to the method reported before [30, 31]. The first intermediate was synthesized by the reaction between 4-bromo-1,8-naphthalic anhydride and *n*-butylamine. Then, the intermediate reacted with diethanolamine to afford BHN. ESI-MS: m/z 357.3 ($M + H^+$). ^1H NMR ($CDCl_3$, 400 MHz): δ (ppm): 0.95 (t, 3H, $J = 8.0$ Hz); 1.41(m, 2H); 1.66 (m, 2H); 2.69 (m, 2H); 3.60 (t, 4H, $J = 5.0$ Hz); 3.86(t, 4H, $J = 5.0$ Hz); 4.08 (t, 2H, $J = 8.0$ Hz); 7.33 (d, 1H, $J = 8.0$ Hz); 7.58 (t, 1H, $J = 8.0$ Hz); 8.38(d, 1 H, $J = 8.0$ Hz); 8.41 (dd, 1H, $J = 8.0$ Hz); 8.84 (dd, 1H, $J = 8.0$ Hz).

BHN (356 mg, 1 mmol) and 3-isocyanatopropyltriethoxysilane (IPTES, 494 mg, 2 mmol) were mixed in anhydrous THF (15 mL) at room temperature. Then the solution was refluxed for 48 h under N_2. After that, the solvent was evaporated, and the crude product was further purified by flash column chromatography (silica gel, petroleum ether/CH_2Cl_2/methanol 50/50/1) to afford 255 mg (30%) of BHN-IPTES as a yellow powder. ESI-MS: m/z 851.5($M + H^+$). ^1H NMR: (400 MHz, $CDCl_3$): δ (ppm) 0.60 (t, 4H, $J = 8.0$ Hz); 0.98 (t, 3H, $J = 8.0$ Hz); 1.21 (m, 18H); 1.45 (m, 2H); 1.58 (m, 4H); 1.70 (m, 2H); 3.13 (m, 4H); 3.73 (t, 2H, $J = 5.0$ Hz); 3.82 (m, 12H); 4.16 (m, 4H); 4.24 (m, 4H); 4.94 (m, 2H); 7.38 (d, 1H, $J = 8.0$ Hz); 7.70 (t, 1H, $J = 8.0$ Hz); 8.45 (d, 1H, J = 8.0 Hz); 8.50 (dd, 1H, $J = 8.0$ Hz); 8.58 (dd, 1H, $J = 8.0$ Hz).

One hundred milligrams of dried Fe_3O_4@SiO_2 nanoparticles and 300 mg (0.35 mmol) of BHN-IPTES were suspended in anhydrous toluene (15 mL). The solution was refluxed for 12 h at 110 °C under N_2 to obtain BHN-Fe_3O_4@SiO_2. The nanoparticles were collected by centrifugation (10,000 rpm) and repeatedly washed with anhydrous ethanol thoroughly. By monitoring the fluorescence of the upper liquid, unreacted organic molecules could be removed completely. Then, the BHN-Fe_3O_4@SiO_2 nanostructure was finally dried under vacuum overnight.

Results and Discussion

Design of BHN-Fe_3O_4@SiO_2

Fe_3O_4@SiO_2 nanoparticle is a promising candidate to construct safe, recyclable, and reusable Fe^{3+} fluorescent sensor due to its low toxicity, high biocompatibility, and convenient recyclability via external magnetic field. Compared with other fluorophores, 1,8-naphthalimide has a large Stokes' shift, long emission wavelength, and convenience to modify with different side-chain and high quantum yield. So, with the introduction of proper side-chain, it can be grafted on the Fe_3O_4@SiO_2 nanoparticle to obtain a safe, recyclable, and reusable Fe^{3+} fluorescent sensor with remarkable fluorescence response.

As is well known, Fe^{3+} can be easily coordinated with O and N atom, so we modified 1,8-naphthalimide with diethanolamine to make the 1,8-naphthalimide possess the ability to detect Fe^{3+} as shown in Fig. 1a. In the diethanolamine, hydroxyethyl and ester-amide moieties were served as a receptor unit. Finally, the modified 1,8-naphthalimide was grafted on the Fe_3O_4@SiO_2 via hydrolysis-condensation reaction between Si $(OEt)_3$ and hydroxyl in the surface of Fe_3O_4@SiO_2 as shown in Fig. 1b.

Structure of BHN-Fe_3O_4@SiO_2

From the TEM image as shown in Fig. 2a, the typical core/shell structure of BHN-Fe_3O_4@SiO_2 is clearly displayed. Although the bare magnetic core is easy to aggregate in liquid, the silica shell on the surface of magnetic nanoparticles would prevent aggregation and improve the dispersibility. The iron oxide nanoparticles have been entrapped in the silica shell successfully and dispersed well. It can also be seen that the overall diameters of core/shell structures are in a narrow distribution of 50 to 60 nm with iron oxide core of 10 nm, which is lower than its superparamagnetic critical size and suitable for using as fluorescent probe's carrier nanoparticle.

Figure 2b shows the XRD powder diffraction patterns of Fe_3O_4, Fe_3O_4@SiO_2, and BHN-Fe_3O_4@SiO_2. The six

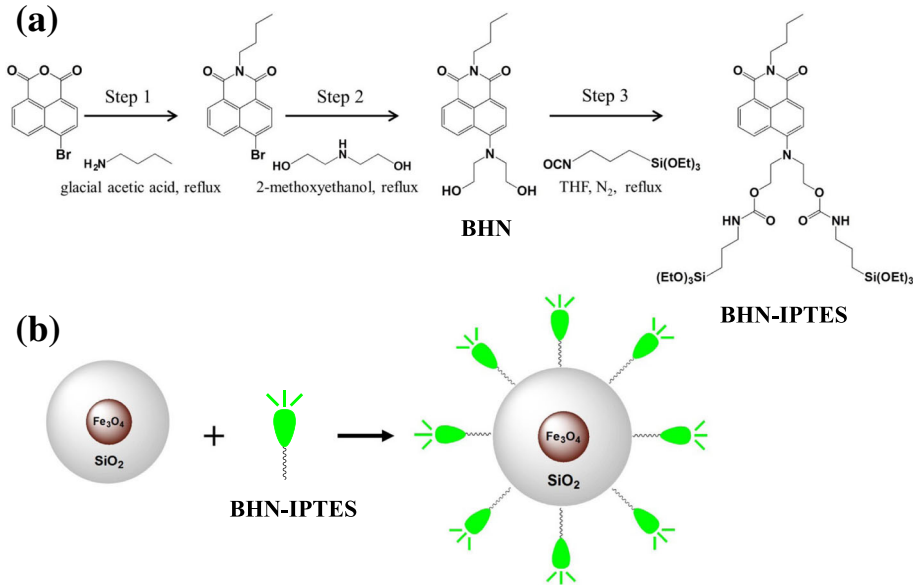

Fig. 1 **a** Synthesis of BHN. **b** Synthesis of BHN-Fe_3O_4@SiO_2

characteristic diffraction peaks of bare Fe_3O_4 can be indexed to 220, 311, 400, 422, 511, and 440 reflections of the magnetite. However, the XRD peaks attributed to Fe_3O_4 have low intensities in Fe_3O_4@SiO_2 and BHN-Fe_3O_4@SiO_2, which implies that the Fe_3O_4 nanoparticles are coated with amorphous silica shell. The silica shell may decrease the relative content of Fe_3O_4 cores and then affect the peak intensities. Also, the broad XRD package is found at a low diffraction angle of 20° to 30° in Fe_3O_4@SiO_2 and BHN-Fe_3O_4@SiO_2, which

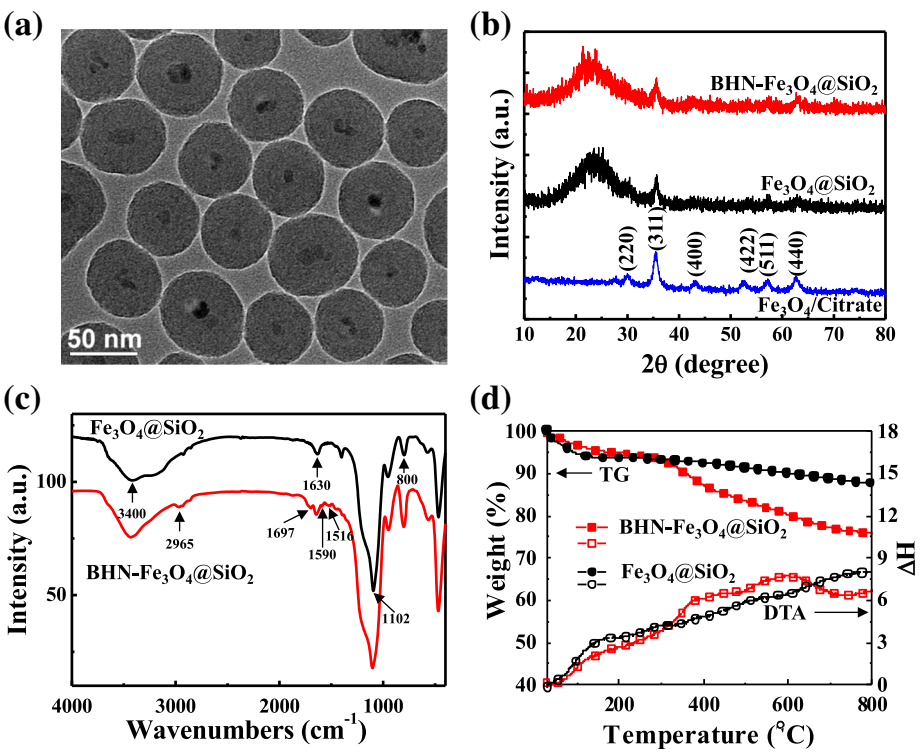

Fig. 2 **a** TEM image of BHN-Fe_3O_4@SiO_2 (the scale bar is 50 nm.). **b** XRD patterns of Fe_3O_4/Citrate, Fe_3O_4@SiO_2, and BHN-Fe_3O_4@SiO_2. **c** FT-IR spectra of Fe_3O_4@SiO_2 and BHN-Fe_3O_4@SiO_2. **d** TG and DTA curves of Fe_3O_4@SiO_2 and BHN-Fe_3O_4@SiO_2

corresponds to the amorphous-state SiO_2 shells surrounding the Fe_3O_4 nanoparticles.

To study the modification condition of BHN-IPTES on the surface of the Fe_3O_4@SiO_2 nanoparticles, its Fourier transform infrared (FT-IR) spectrum is measured. As shown in Fig. 2c, both two curves exhibited the typical vibration band of –OH stretching on silanol at 3400 to 3500 cm^{-1} and 1000 to 1200 cm^{-1} [32]. It indicates that not all the silanol on Fe_3O_4@SiO_2 nanoparticles have been covalently modified. The band at 1630 cm^{-1} represents the bending mode of –OH vibrations [33]. The bands centered at 1109 (*vas*) and 800 cm^{-1} can be attributed to the siloxane (-Si-O-Si-) [34]. The above peaks indicate the existence of silica shell. The additional peaks at 2965 and 2934 cm^{-1} were found in BHN-Fe_3O_4@SiO_2, corresponding to the –CH vibration of aliphatic and aromatic groups [32, 35]. The band at 1697, 1590, and 1516 cm^{-1} of BHN-Fe_3O_4@SiO_2 comes from the bending vibrations of $-CH_3$ from the BHN part [36]. These results demonstrate the presence of the organic molecule in the magnetic material BHN-Fe_3O_4@SiO_2.

The superparamagnetic property of the magnetic nanoparticles plays a vital role for its biological application. Additional file 1: Figure S1 shows the magnetization curve of BHN-Fe_3O_4@SiO_2 which was measured by a vibrating sample magnetometer in the range from − 15,000 to 15,000 Oe at 300 K. The result was consistent with the conclusion that the diameter of magnetic Fe_3O_4 nanoparticles less than 30 nm is usually superparamagnetic at room temperature [37]. The saturation magnetization

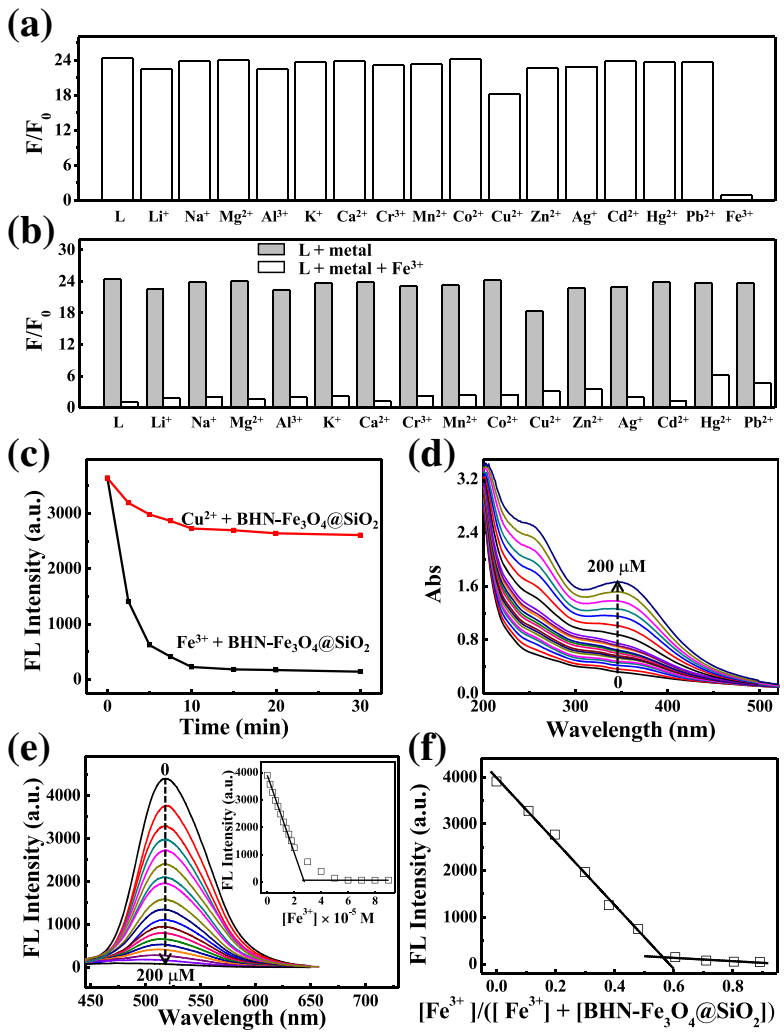

Fig. 3 **a** Fluorescence responses of BHN-Fe_3O_4@SiO_2 with various cations. Excitation wavelength was 415 nm. Spectra were recorded every 2 min after adding metal ions. **b** Competition of Fe^{3+}-BHN-Fe_3O_4@SiO_2 towards cations. Fluorescent emission change of BHN-Fe_3O_4@SiO_2 (0.2 g/L) upon addition of metal ions (each metal ion is 5×10^{-5} M) in CH_3CN/H_2O 1:1 (HEPES buffer pH 7.36) at room temperature. **c** Time responses of BHN-Fe_3O_4@SiO_2 with Fe^{3+} and Cu^{2+}. **d** UV-Vis titrations of BHN-Fe_3O_4@SiO_2 (0.2 g/L) with Fe^{3+}. **e** Fluorescence titration of BHN-Fe_3O_4@SiO_2 (0.2 g/L) with Fe^{3+}. Inset: the fluorescence intensities at 518 nm at various concentrations of Fe^{3+}. **f** Job's plot of BHN-Fe_3O_4@SiO_2 with Fe^{3+}

value for synthesized BHN-Fe_3O_4@SiO_2 is about 4.02 emu/g. More importantly, from the hysteresis loop of BHN-Fe_3O_4@SiO_2 nanostructure, it can be found that it exhibited superparamagnetic properties, and no coercive force was observed in the hysteresis loop. This phenomenon was due to the fact that the magnetite core has a small diameter around 10 nm. At the same time, the silica shell prevents the aggregation of magnetite core. So, the BHN-Fe_3O_4@SiO_2 nanostructure can further show good dispersibility.

Fluorescence Response of BHN-Fe_3O_4@SiO_2

To verify the fluorescence response of BHN-Fe_3O_4@SiO_2 for various metal ions, the fluorescence measurements were carried out in CH_3CN/H_2O 1:1 (*v*/*v*) solution at pH 7.36 in HEPES buffer. The concentration of BHN-Fe_3O_4@SiO_2 is 0.2 g/L (corresponding to the free organic molecule was about 3.34×10^{-5} M, according to the TGA, see Fig. 2d), and the various metal ions Ag^+, Al^{3+}, Ca^{2+}, Cd^{2+}, Co^{2+}, Cr^{3+}, Cu^{2+}, Hg^{2+}, K^+, Li^+, Mg^{2+}, Mn^{2+}, Na^+, Pb^{2+}, Zn^{2+}, and Fe^{3+} (all as their perchlorates salts) were 5.0×10^{-5} M. As shown in Fig. 3a, a significant fluorescence quenching was observed when adding Fe^{3+}, but no significant decrease of fluorescent intensity in the same conditions was detected if adding other metal ions except Cu^{2+}. Cu^{2+} would cause slight fluorescence quenching and response in 20 min. However, at the same detecting conditions, Fe^{3+} causes a response in 2 min and quench obviously in 5 min (Fig. 3c). The absorption spectra of BHN-Fe_3O_4@SiO_2 (0.2 g/L) in the presence of various concentrations of Fe^{3+} (0 to 200 μM) were investigated, as shown in Fig. 3d. When Fe^{3+} was added gradually, the absorbance of BHN-Fe_3O_4@SiO_2 at 250 and 350 nm gradually increases, which indicated that BHN-Fe_3O_4@SiO_2 nanostructure coordinated with Fe^{3+} gradually.

Then, a fluorescence titration with $Fe(ClO_4)_3$ in CH_3CN/H_2O 1:1 (*v*/*v*) was applied to understand the combination of BHN-Fe_3O_4@SiO_2 towards Fe^{3+} ions. As illustrated in Fig. 3e, the fluorescence emission of BHN-Fe_3O_4@SiO_2 (0.2 g/L) decreases gradually when various concentrations (0 to 100 μM) of Fe^{3+} were added in CH_3CN/H_2O 1:1 (*v*/*v*) HEPES buffer, which indicates that BHN-Fe_3O_4@SiO_2 nanostructure coordinated with Fe^{3+} to form the complex quantitatively. Fluorescence titration experiment suggests that the association constant logβ for Fe^{3+} binding to BHN-Fe_3O_4@SiO_2 is calculated to be 8.23. A linear increasing of fluorescence from the BHN-Fe_3O_4@SiO_2 nanostructure was observed upon the addition of Fe^{3+} between 0 and 20 μM, and the limit of detection of BHN-Fe_3O_4@SiO_2 to Fe^{3+} was found by 1.25×10^{-8} M under the fluorimetric assay. The fluorescence titration and Job plot results suggested a 1:1 binding ration for Fe^{3+} with BHN-Fe_3O_4@SiO_2 (Fig. 3f). The results of cation competitive experiments are depicted in Fig. 3b, and it could be found that the selectivity and sensitivity of BHN-Fe_3O_4@SiO_2 to Fe^{3+} are not influenced by other metal ions.

Here, the remarkable decrease of fluorescence intensity can be explained as follow: The fluorescence intensity of BHN-Fe_3O_4@SiO_2, which is excited at a 415 nm lamp, exhibits the high fluorescence at 518 nm due to the 1,8-naphthalimide which has a big conjugated system. In addition, electron donating group in the structure influences the fluorescent of

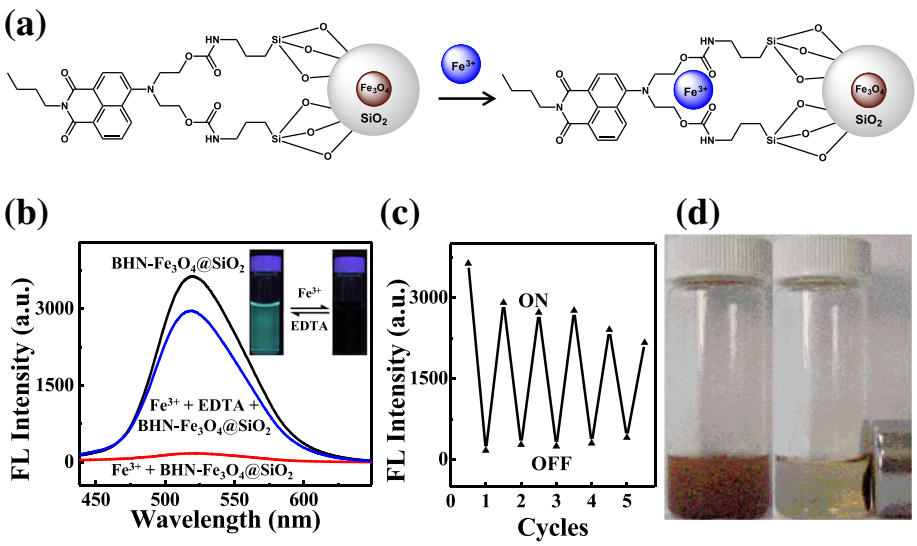

Fig. 4 **a** Schematic show of BHN-Fe_3O_4@SiO_2 with Fe^{3+}. **b** Reversibility of BHN-Fe_3O_4@SiO_2 towards Fe^{3+}. Inset: the photograph of BHN-Fe_3O_4@SiO_2 with Fe^{3+} by treatment of EDTA (2.5×10^{-5} M) under 415-nm UV light. **c** Plot of the fluorescence of BHN-Fe_3O_4@SiO_2 (0.2 g/L) with alternate adding of 2.5×10^{-5} M Fe^{3+} ("off") and EDTA ("on"). **d** BHN-Fe_3O_4@SiO_2 (0.2 g/L) was dispersed to an external magnet in CH_3CN/H_2O 1:1 (HEPES buffer pH 7.36)

system at the same time. When stably chelated with Fe^{3+} by the O atom and N atom on the four-position of 1,8-naphthalimide, the electron or energy transfer between the metal cation and the fluorophore produce an electronic absorption effect, so as to make the fluorescence quenching [38] (Fig. 4a).

The fluorescence quenching by adding Fe^{3+} to the solution of BHN-Fe_3O_4@SiO_2 was fully reversible. When adding EDTA (2.5×10^{-5} M) to the Fe^{3+}-BHN-Fe_3O_4@SiO_2 system, the fluorescence intensity was almost restored to the original level of BHN-Fe_3O_4@SiO_2 (Fig. 4b). Further, reusability was evaluated by repeatedly adding Fe^{3+}-EDTA cycles into the system, with the change of BHN-Fe_3O_4@SiO_2 fluorescence intensity being recorded after each step, and the corresponding data are shown in Fig. 4c. It is clear that the BHN-Fe_3O_4@SiO_2 exhibits excellent reusability because only the rare loss in BHN-Fe_3O_4@SiO_2 sensitivity towards Fe^{3+} was observed after five repeated Fe^{3+}-EDTA cycles. As a result of its magnetic property, BHN-Fe_3O_4@SiO_2 had a reversal magnetic responsibility. As shown in Fig. 4d, it could be easily separated from the dispersion (0.2 g/L) after 10 min by placing a magnet closed to the dispersion, then redispersed by mild agitation when the magnet was removed. This magnetic separation capability and the recognition property of BHN-Fe_3O_4@SiO_2 nanostructure provide a simple and efficient route to separate Fe^{3+} rather than through filtration approach. More important is that the reversal magnetic responsibility of BHN-Fe_3O_4@SiO_2 nanostructure would be a key factor when evaluating their recyclability [39]. Combined with its magnetic property, it is demonstrated that BHN-Fe_3O_4@SiO_2 was considerably applicable in the biological system as an efficient inorganic-organic hybrid sensor for Fe^{3+}.

For the biological application, it is critically important that the sensor should be suitable for measuring specific metal ion in the physiological pH range. As shown in Fig. 5a, the fluorescence intensities of BHN-Fe_3O_4@SiO_2 with/without Fe^{3+} at various pH values were investigated. The fluorescence intensity of BHN-Fe_3O_4@SiO_2 slightly decreases when adding Fe^{3+} under acidic conditions, since protonation of N atom on the four-position of 1,8-naphthalimide leads to a weak coordination ability of Fe^{3+}. Then, a dramatic fluorescence change for Fe^{3+}-BHN-Fe_3O_4@SiO_2 system was found when pH was at neutral pH and under weakly alkaline conditions. Here, BHN-Fe_3O_4@SiO_2 exhibits excellent Fe^{3+} sensing abilities when the pH is in the range of 5.84 to 10.52, which indicates that BHN-Fe_3O_4@SiO_2 is an expecting probe to be applied in those complicated environments or biological systems.

To further demonstrate the ability of BHN-Fe_3O_4@SiO_2 to detect Fe^{3+} in living systems, we carried on an experiment in live HeLa cells. First of all, we investigated the cell

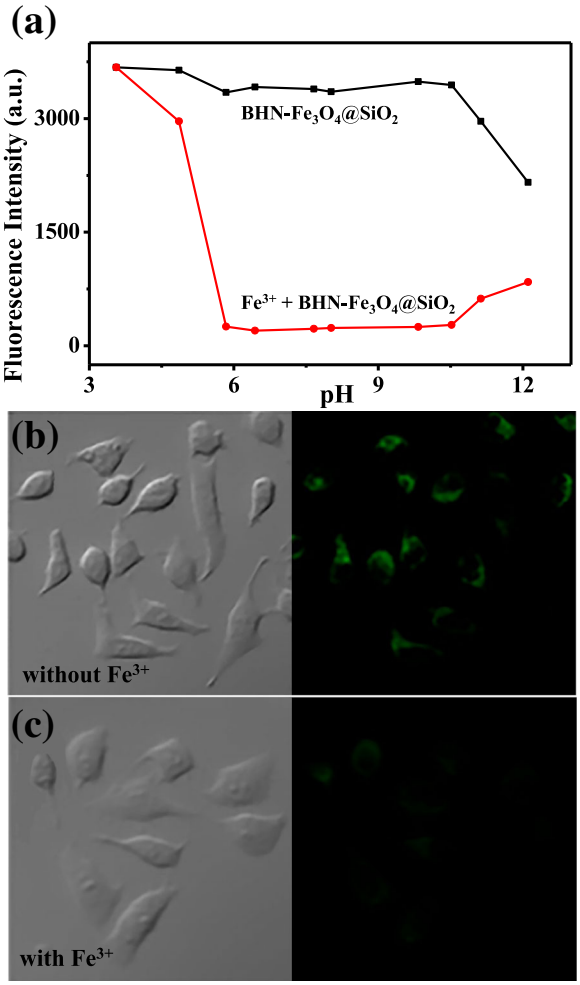

Fig. 5 **a** Fluorescence intensities of BHN-Fe_3O_4@SiO_2 and Fe^{3+}-BHN-Fe_3O_4@SiO_2 at various pH values at room temperature. CH_3CN/H_2O 1:1, $\lambda_{ex} = 415$ nm. **b** Bright field image and fluorescence image of the HeLa cells with BHN-Fe_3O_4@SiO_2. (**c**) Bright field image and fluorescence image of the HeLa cells with BHN-Fe_3O_4@SiO_2 and Fe^{3+}

viability of BHN-Fe_3O_4@SiO_2 and Fe^{3+}-BHN-Fe_3O_4@SiO_2 using the MTT assay. HeLa cells were incubated with BHN-Fe_3O_4@SiO_2 in RPMI-1640 for 0.5 h at 37 °C, and then $Fe(ClO_4)_3$ was added for incubation for 0.5 h. Then, the confocal fluorescence images of the HeLa cells were observed, and it shows excellent staining capacity when the concentration of the sensor and $Fe(ClO_4)_3$ is up to 0.2 g/L and 5×10^{-5} M. Then, we conducted fluorescence microscopy experiment to investigate its higher gradation of application in complex biological systems. As shown in Fig. 5b, HeLa cells were grown on 12 orifice plate at 37 °C and in 5% CO_2 atmosphere for 24 h, then treated with BHN-Fe_3O_4@SiO_2 (0.2 g/L) and incubated for 0.5 h, and the cells showed strong green fluorescence. Then, the cells were treated with 5×10^{-5} M $Fe(ClO_4)_3$. After 0.5 h, we did observe the fluorescent remarkably decreased (Fig. 5c).

Thus, we can draw a conclusion that BHN-Fe_3O_4@SiO_2 can be used to image Fe^{3+} in living cells.

Conclusion

In summary, a novel multifunctional fluorescent probe BHN-Fe_3O_4@SiO_2 nanostructure for Fe^{3+} was successfully designed and synthesized. The probe BHN-Fe_3O_4@SiO_2 can selectively respond to Fe^{3+} with fluorescence quenching and efficient separation of Fe^{3+} with external magnetic field. The constituted on-off type fluorescence monitoring system indicates that the probe could be reversed back and reused. At the same time, the probe has been successfully applied to quantitatively detect Fe^{3+} with low detection limits. Furthermore, the BHN-Fe_3O_4@SiO_2 nanostructure probe is successfully used to detect Fe^{3+} in living HeLa cells, which shows its great potential in bioimaging detection.

Additional file

Additional file 1: Figure S1. a Magnetization curve of BHN-Fe_3O_4@SiO_2. **b** UV-Vis spectra of BHN-IPTES, Fe_3O_4@SiO_2, and BHN-Fe_3O_4@SiO_2. (PDF 57 kb)

Abbreviations

BHN: *N*-butyl-4-bis(2-hydroxyethyl) amino-1,8-naphthalimide; EDTA: Ethylenediaminetetraacetic acid; FT-IR: Fourier transform infrared; IPTES: 3-Isocyanatopropyl-triethoxysilane; TEM: Transmission electron microscopy; TEOS: Tetraethyl orthosilicate; TGA: Thermal gravimetric analysis; THF: Tetrahydrofuran; XRD: X-ray powder diffraction

Acknowledgements

This study was supported by the NSFC (NO. 20931003, 20771048) and the Specialized Research Funds for the Doctoral Program of Higher Education (20110211130002).

Availability of data and materials

All reagents are purchased commercially, and tetrahydrofuran (THF) and toluene were used after dehydration. Other chemicals were used as received without further purification. Thermal gravimetric analysis (TGA) was performed on a PE Diamond TG/DTA/SPAECTRUN ONE thermal analyzer up to 800 °C at a heating rate of 10 °C min^{-1} in an N_2 atmosphere. Transmission electron microscopy (TEM) (Tecnai G^2 F30, 300 kV, FEI Company, OR, USA) was used to characterize the materials. X-ray diffraction (XRD) pattern of the synthesized products was recorded with a Rigaku D/MAX 2400 X-ray diffractometer (Tokyo, Japan) using Cu *Ka* radiation ($\lambda = 0.154056$ Å). The scan range (2θ) was from 10° to 80°. Solid-state infrared (IR) using diffuse reflectance infrared Fourier transform (DRIFT) spectroscopy was performed in the 400 to 4000 cm^{-1} region using a Bruker Vertex 70 V (Bremen, Germany) and IR-grade KBr (Sigma-Aldrich Corporation, St. Louis, MO, USA) as the internal standard. ^1H NMR was measured on a Bruker DRX 400 spectrometer in a $CDCl_3$ solution with TMS as the internal standard. Chemical shift multiplicities are reported as s = singlet, t = triplet, q = quartet, and m = multiplet. Mass spectra were recorded on a Bruker Daltonics esquire6000 mass spectrometer. UV absorption spectra were recorded on Varian Cary 100 spectrophotometer (Palo Alto, CA, USA) using quartz cells of 1.0-cm path length. Fluorescence measurements were made on a Hitachi F-7000 spectrophotometer (Tokyo, Japan) and a Shimadzu RF-540 spectrofluorophotometer (Chorley, UK) equipped with quartz cuvettes of 1.0-cm path length with a xenon lamp as the excitation source. An excitation and emission slit of 5.0 nm was used for the measurements in the solution state. All pH measurements were made with a pH-10C digital pH meter. All spectrophotometric titrations were performed with a suspension of the sample dispersed in CH_3CN/H_2O (1:1, HEPES buffer pH 7.36).

Authors' contributions

XZ supervised and participated in all the studies and wrote this paper. YW conceived the study and participated in its design. QP participated in the cell experiment. WL participated in the revision of the manuscript. All authors read and approved the final manuscript.

Competing interests

The authors declare that they have no competing interests.

Publisher's Note

Author details

[1]Key Laboratory of Nonferrous Metals Chemistry and Resources Utilization of Gansu Province, State Key Laboratory of Applied Organic Chemistry, College of Chemistry and Chemical Engineering, Lanzhou University, Lanzhou 730000, China. [2]Department of Pathogenic Biology, School of Basic Medical Sciences, Lanzhou University, Lanzhou 730000, China.

Received: 12 November 2017 Accepted: 30 November 2017
Published online: 19 December 2017

References

1. Lippard SJ, Berg JM (1994) Principles of bioinorganic chemistry. University Science Books, Mill Valley, California, pp 105–136
2. Kaim W, Schwederski B, Klein A (2013) Bioinorganic chemistry: inorganic elements in the chemistry of life: an introduction and guide, 2nd edn. John Wiley & Sons Inc., Chichester, pp 139–160
3. Yoon TJ, Kim JS, Kim BG, Yu KN, Cho MH, Lee JK (2005) Multifunctional nanoparticles possessing a "magnetic motor effect" for drug or gene delivery. Angew Chem Int Ed 44(7):1068–1071
4. Beutler E (2004) "Pumping" iron: the proteins. Science 306(5704):2051–2053
5. Dai S, Schwendtmayer C, Schürmann P, Ramaswamy S, Eklund H (2000) Redox signaling in chloroplasts: cleavage of disulfides by an iron–sulfur cluster. Science 287(5453):655–658
6. Goldberg AV, Molik S, Tsaousis AD, Neumann K, Kuhnke G, Delbac F et al (2008) Localization and functionality of microsporidian iron-sulphur cluster assembly proteins. Nature 452(7187):624–628
7. Kaplan CD, Kaplan J (2009) Iron acquisition and transcriptional regulation. Chem Rev 109(10):4536–4552
8. Theil EC, Goss DJ (2009) Living with iron (and oxygen): questions and answers about iron homeostasis. Chem Rev 109(10):4568–4579
9. Atkinson A, Winge DR (2009) Metal acquisition and availability in the mitochondria. Chem Rev 109(10):4708–4721
10. Beutler E (2007) Iron storage disease: facts, fiction and progress. Blood Cells Mol Dis 39(2):140–147
11. Sahoo SK, Sharma D, Bera RK, Crisponi G, Callan JF (2012) Iron(III) selective molecular and supramolecular fluorescent probes. Chem Soc Rev 41(21): 7195–7227
12. Lunvongsa S, Oshima M, Motomizu S (2006) Determination of total and dissolved amount of iron in water samples using catalytic spectrophotometric flow injection analysis. Talanta 68(3):969–973
13. Ferreira SLC, Souza AS, Brandao GC, Ferreira HS, dos Santos WNL, Pimentel MF et al (2008) Direct determination of iron and manganese in wine using the reference element technique and fast sequential multi-element flame atomic absorption spectrometry. Talanta 74(4):699–702
14. Wilhartitz P, Dreer S, Krismer R, Bobleter O (1997) High performance ultra trace analysis in molybdenum and tungsten accomplished by on-line coupling of ion chromatography with simultaneous ICP-AES. Microchim Acta 125:45–52
15. Gupta NR, Mittal S, Kumar S, Ashok Kumar SK (2008) Potentiometric studies of N,N'-Bis(2-dimethylaminoethyl)-N,N'-dimethyl-9,10-anthracenedimethanamine as a chemical sensing material for Zn(II) ions. Mater Sci Eng C 28(7):1025–1030
16. Carter KP, Young AM, Palmer AE (2014) Fluorescent sensors for measuring metal ions in living systems. Chem Rev 114(8):4564–4601
17. Hyman LM, Franz KJ (2012) Probing oxidative stress: small molecule fluorescent sensors of metal ions, reactive oxygen species, and thiols. Coordin Chem Rev 256:2333–2356

18. Li CY, Zou CX, Li YF, Tang JL, Weng C (2014) A new rhodamine-based fluorescent chemosensor for Fe^{3+} and its application in living cell imaging. Dyes Pigments 104:110–115
19. Wang R, Yu F, Liu P, Chen L (2012) A turn-on fluorescent probe based on hydroxylamine oxidation for detecting ferric ion selectively in living cells. Chem Commun 48(43):5310–5312
20. Au-Yeung HY, Chan J, Chantarojsiri T, Chang CJ (2013) Molecular imaging of labile iron(II) pools in living cells with a turn-on fluorescent probe. J Am Chem Soc 135(40):15165–15173
21. Marshall M, Draney D, Sevick-Muraca E, Olive DM (2010) Single-dose intravenous toxicity study of IRDye 800CW in Sprague-Dawley rats. Mol Imaging Biol 12(6):583–594
22. Han WS, Lee HY, Jung SH, Lee SJ, Jung JH (2009) Silica-based chromogenic and fluorogenic hybrid chemosensor materials. Chem Soc Rev 38(7):1904–1915
23. Zheng J, Xiao C, Fei Q, Li M, Baojun W, Guodong F et al (2010) A highly sensitive and selective fluorescent Cu^{2+} sensor synthesized with silica nanoparticles. Nanotechnology 21(4):045501
24. Meng Q, Zhang X, He C, He G, Zhou P, Duan C (2010) Multifunctional mesoporous silica material used for detection and adsorption of Cu^{2+} in aqueous solution and biological applications in vitro and in vivo. Adv Funct Mater 20(12):1903–1909
25. Taboada E, Solanas R, Rodríguez E, Weissleder R, Roig A (2009) Supercritical-fluid-assisted one-pot synthesis of biocompatible Core(γ-Fe_2O_3)/Shell(SiO_2) Nanoparticles as high Relaxivity T_2-contrast agents for magnetic resonance imaging. Adv Funct Mater 19(14):2319–2324
26. Zhang L, Wang Y, Tang Y, Jiao Z, Xie C, Zhang H et al (2013) High MRI performance fluorescent mesoporous silica-coated magnetic nanoparticles for tracking neural progenitor cells in an ischemic mouse model. Nano 5(10):4506–4516
27. Zheng J, Dong Y, Wang W, Ma Y, Hu J, Chen X et al (2013) In situ loading of gold nanoparticles on Fe_3O_4@SiO_2 magnetic nanocomposites and their high catalytic activity. Nano 5(11):4894–4901
28. Nigam S, Barick KC, Bahadur D (2011) Development of citrate-stabilized Fe_3O_4 nanoparticles: conjugation and release of doxorubicin for therapeutic applications. J Magn Magn Mater 323(2):237–243
29. Stöber W, Fink A, Bohn E (1968) Controlled growth of monodisperse silica spheres in the micron size range. J Colloid Interface Sci 26(1):62–69
30. Wang J, Bi C, Yuan B, Li Z, Qiao W, Luan J (2006) Design and synthesis of fluorescent non-ionic surfactants. Petrochem Technol 35(5):464–468
31. Guo X, Zhu B, Liu Y, Zhang Y, Jia L, Qian X (2006) Synthesis and properties of N-Butyl-4-(aza-15-crown-5)-1,8-naphthalimide as a fluorescent probe. Chinese J Org Chem 26(4):504–507
32. Mu L, Shi W, Chang JC, Lee S-T (2008) Silicon nanowires-based fluorescence sensor for cu(II). Nano Lett 8(1):104–109
33. Murthy RSS, Leyden DE (1986) Quantitative determination of (3-aminopropyl) triethoxysilane on silica gel surface using diffuse reflectance infrared Fourier transform spectrometry. Anal Chem 58(6):1228–1233
34. Kim E, Kim HJ, Bae DR, Lee SJ, Cho EJ, Seo MR et al (2008) Selective fluoride sensing using organic-inorganic hybrid nanomaterials containing anthraquinone. New J Chem 32(6):1003–1007
35. Song C, Zhang X, Jia C, Zhou P, Quan X, Duan C (2010) Highly sensitive and selective fluorescence sensor based on functional SBA-15 for detection of Hg^{2+} in aqueous media. Talanta 81:643–649
36. Sasithorn J, Wiwattanadate D, Sangsuk S (2010) Utilization of fly ash from power plant for adsorption of hydrocarbon contamination in water. J Met Mater Miner 20(1):5–10
37. Lin Y-S, Haynes CL (2009) Synthesis and characterization of biocompatible and size-tunable multifunctional porous silica nanoparticles. Chem Mater 21(17):3979–3986
38. Sarkar M, Banthia S, Samanta A (2006) A highly selective "off–on" fluorescence chemosensor for Cr(III). Tetrahedron Lett 47(43):7575–7578
39. Wang Y, Peng X, Shi J, Tang X, Jiang J, Liu W (2012) Highly selective fluorescent chemosensor for Zn2+ derived from inorganic-organic hybrid magnetic core/shell Fe3O4@SiO2 nanoparticles. Nanoscale Res Let 7(1):86